

Article

Synergistic Occlusion of Doxorubicin and Hydrogels in CaCO₃ Composites for Controlled Drug Release

Ya-Xin Li and Yuan Jiang * 

College of Materials, Fujian Key Laboratory of Advanced Materials, Higher Educational Key Laboratory for Biomedical Engineering of Fujian Province, Xiamen University, Xiamen 361005, China

* Correspondence: yuan.jiang@xmu.edu.cn

Abstract: Extensive exploration is required to deploy mineralization as a tool to develop low-cost yet efficient sustained drug release systems. Unlike previous studies which directly incorporated drug components in mineralized products, we propose an emerging approach to synthesizing drug-loaded CaCO₃ composites, relying on the synergistic occlusion of the molecular solutions comprising both the alginate hydrogel matrices and the associated drug (doxorubicin) in the course of mineralization. Independent tools including a scanning electron microscope and adsorption isotherm were employed to characterize the lyophilized composites, which led to the conclusion that the anticancer drug doxorubicin (DOX) was uniformly dispersed in the hydrogel matrices as a molecular solution. The occlusion strategy led to CaCO₃-based composites with high loads and sustained and pH-responsive release of DOX. Considering many drug molecules can form molecular solutions with polymeric components, we find that the synergistic occlusion can become a general approach to designing smart drug delivery systems.

Keywords: mineralization; doxorubicin; occlusion; synergy; hydrogel



Citation: Li, Y.-X.; Jiang, Y. Synergistic Occlusion of Doxorubicin and Hydrogels in CaCO₃ Composites for Controlled Drug Release. *Crystals* **2023**, *13*, 132. <https://doi.org/10.3390/cryst13010132>

Academic Editor: Changquan Calvin Sun

Received: 15 October 2022
Revised: 16 December 2022
Accepted: 9 January 2023
Published: 11 January 2023



Copyright: © 2023 by the authors. Licensee MDPI, Basel, Switzerland. This article is an open access article distributed under the terms and conditions of the Creative Commons Attribution (CC BY) license (<https://creativecommons.org/licenses/by/4.0/>).

1. Introduction

Calcium carbonate (CaCO₃) represents a type of pH-responsive drug carrier which has been extensively employed in drug release systems because of its low cost, simple production, intrinsic biocompatibility, and proper biodegradability [1]. The mineral is stable under neutral and basic pH ranges and will be decomposed into Ca²⁺ and HCO₃[−] when the local aqueous phase turns acidic in inflamed and cancerous tissues, causing spontaneous release of drug compounds for chemotherapy. The drug-CaCO₃ hybrids can be established by the passivate adsorption of drug (macro)molecular compounds on mineral surfaces, and therefore, the relatively weak binding strength in between may cause inadequate sustained release or targeting. The nanosized CaCO₃ particles [2–4], porous CaCO₃ scaffolds [5–8], mesocrystals [9], and hollow microparticles [10,11] featured by large surface areas become promising candidates for high drug load and efficient release performance. Nevertheless, the synthetic routes to these CaCO₃-drug composite particles can be sophisticated and require strict experimental conditions. Development of an efficient approach to CaCO₃-based drug composites is therefore anticipated to achieve sufficient loads for on-demand sustained drug release.

Biomineralization provides us a general strategy for the occlusion of organic compounds in inorganic matrices [12]. A growing number of mineralization studies have reported the direct occlusion of organic components in CaCO₃ crystals. These organics, spanning across organic molecules [13–15], charged and non-charged macromolecules [16–18], micelles [19,20], and nanoparticles [21], are distinct in chemistry and structural forms, which indicates that their occlusion in CaCO₃ crystals can be a general approach to growing inorganic-organic composites [22,23]. For instance, a drug compound—doxorubicin (DOX)—can be uniformly occluded in single crystalline calcite for the establishment of a

controlled drug release system for cancer cell treatment [13,24]. However, it is worth noting that not all organics can be directly occluded in CaCO_3 crystals in the course of mineralization. Moreover, the direct occlusion of organics in CaCO_3 crystals always accompanies the occurrence of lattice distortions in the course of mineralization [25]. Hence, a synergistic occlusion strategy remains to be required for the controllable generation of CaCO_3 -based drug release systems.

Indeed, the synergistic occlusion of multiple organic components is a universal strategy that can be deployed in the formation of biogenic and synthetic minerals [23,26]. The synergy of multiple organic constituents is responsible not only for the evolution of specific hierarchical architectures [26,27] but for the reconciliation of multiple properties [28]. For instance, glycoproteins, together with silk fibroin-like media and chitinous constituents, are responsible for the generation of brick-and-mortar structures in mollusk shells, which show remarkable strength and resilience [29]. This synergistic principle of biomineralization has been employed to design synthetic minerals that can occlude a relatively high level of functional constituents, such as nano-sized particles and organic compounds [23,30]. Particularly, molecular association is an effective approach to the synergistic occlusion of the constituents which cannot be incorporated in CaCO_3 crystals solely. For instance, an insoluble recombinant biomineralization protein, namely perlucin, was bound to soluble green fluorescent proteins for the associated occlusion in calcitic crystals [31]. Another study reported that molecular interactions between amino acids and dye molecules favor the occlusion of dye molecules in CaCO_3 crystals [32]. Though efficient occlusion of the organics in mineralized products could be achieved in the abovementioned studies, little remains known about versatile guidance for screening proper molecular combinations for synergistic occlusion.

Alternatively, hydrogel-mediated mineralization [33] is deemed a universal approach for the synergistic occlusion of both hydrogel networks and the associated nanoparticles or organic compounds in the mineralized composites [34–36]. A sufficient gel strength can withstand crystallization pressure [33], which leads to the simultaneous occlusion of both gelled frameworks and the adhered functional components. Therefore, intimate association of the hydrogels and the functional components can introduce the non-intrinsic properties to the CaCO_3 crystals without considering the structural discrepancy between the dopants and the inorganic matrices. To our knowledge, this synthetic strategy of synergistic occlusion has not been applied to the development of drug-loaded CaCO_3 composites, the success of which can reward us with an emerging material engineering route to drug delivery systems with sufficient drug loads and delivery efficiency.

Herein, we report on mineralization-occluded, DOX-loaded alginate hydrogels in the prismatic CaCO_3 composites with sufficient drug load and sustained release. Multiple microscopic tools were employed to disclose the spatial distribution of the DOX constituents in the drug-loaded composites. Both the synthetic composites and lyophilized DOX-alginate hydrogels were characterized to confirm that the good affinity between the DOX and alginate components could lead to the dispersed form of the drug in alginate hydrogels. Furthermore, an adsorption isotherm was performed to confirm the DOX components were dispersed in an alginate hydrogel as a molecular solution, which guaranteed their synergistic occlusion in the DOX- CaCO_3 -alginate composites and sufficient drug load in the course of mineralization. Finally, the *in vitro* release properties of the DOX- CaCO_3 -alginate composites at different pH values were evaluated systematically.

2. Experimental Section

2.1. Materials

Cocoons of the *Bombyx mori* silkworm were purchased from Fu'an Cocoon Ltd. (Dongtai, Jiangsu, China), and the degumming of the *Bombyx mori* silk fibroin (SF) and preparation of regenerated SF aqueous solutions were conducted following the established procedure [37]. Calcium chloride (powders, AR), NH_4HCO_3 (powders, AR), acetic acid ($\geq 99.8\%$, AR), and ethanol ($\geq 99.8\%$, AR) were purchased from Sinopharm Chemical

Reagent (Shanghai, China). Doxorubicin hydrochloride (powders, 98%), chitosan (average $M_w = 3.0 \times 10^5 \text{ g mol}^{-1}$, viscosity: 800–2000 CP, deacetylation degree: 95%), agarose (powders, type I), and poly(dl-aspartic acid) solutions (PAsp; average $M_w = 2.0 - 11.0 \times 10^3 \text{ g mol}^{-1}$) were purchased from Sigma-Aldrich Co. Ltd. (Shanghai, China). Alginate (powders, CP) was purchased from Xilong Scientific (Beijing, China). All chemicals were purchased and used as received without further purification if not specified. Degassed purified water was obtained from a Direct-Q 3UV water purification system and boiled for 0.5 h to remove CO_2 before use.

2.2. Growth of Seed Layers

Chitosan thin films were used as the substrates for CaCO_3 mineralization. First, a volume of 30 μL 1 wt% chitosan-acetic acid solution was dipped on a clean cover glass (1.0 cm \times 1.0 cm, pretreated with Piranha solution) followed by a spin-coating process using a spin rate at 5000 rpm for 1 min. Then, the substrates were immersed in a volume of 4 mL 20 mM CaCl_2 aqueous solution in the presence of 0.01 g L^{-1} PAsp as the additive in a closed desiccator. The mineralization was performed by a standard gas diffusion method based on the decomposition of NH_4HCO_3 for 24 h. Subsequently, the substrates, together with the hybrid thin films, were removed and rinsed twice with degassed purified water before being used for characterization or overgrowth. Detailed information can be found elsewhere [38,39].

2.3. Deposition of Alginate Hydrogel Layers on Seed Layers

In this work, the alginate solution was mixed with the DOX solution beforehand, where the concentrations of the alginate and DOX were 2.0 wt% and 0.2 g L^{-1} , respectively. A 30 μL solution was dipped on the seed layer followed by a spin-coating process using a spin rate at 1500 rpm for 10 s. A calcium chloride solution was employed for gelation. The alginate-coated seed layers were immersed in 20 mM calcium chloride solution for 4 h before being immersed in water for 1 min to remove the excess calcium chloride solution.

2.4. Overgrowth

The hydrogel-covered seed layers were carefully positioned at the bottom of plastic petri dishes containing a volume of 4 mL CaCl_2 -SF-DOX solution for the growth of overlayers. Growth of the overlayers was conducted in 20 mM CaCl_2 solutions containing 0.2 wt% SF and 0.2 g L^{-1} DOX via the standard gas diffusion method mentioned in the growth of seed layers. Mineralization was performed in ambient conditions for 48 h.

2.5. Isothermal Adsorption of DOX

A quantity of 0.02 g (m_0) lyophilized sodium alginate hydrogels was added into 6 mL (V_0) DOX solutions at concentrations of 5, 10, 20, 40, 60, 80, 100, 120, 140, 160, 180, and 200 mg L^{-1} (c_0) and was kept in the dark for 48 hrs for DOX adsorption. Here, the pH value of the DOX solution was adjusted to 5 with hydrochloric acid (0.1 mol L^{-1}) before use. An ultraviolet-visible (UV-vis) spectrophotometry method was used to determine the concentration of DOX according to the Beer-Lambert law, where the absorbance of the DOX solution (6, 9, 12, 15, and 18 $\mu\text{g mL}^{-1}$) at 480 nm was measured to draw the standard curve (Figure S4). The adsorption capacity (q_e) of the DOX in the alginate gels was calculated according to the following equation. The adsorption capacity (q_e) of the DOX in the agarose gels was measured with the same method. The adsorption capacity (q_e) at different DOX equilibrium concentrations (c_e) was plotted into isothermal adsorption curves:

$$W_0 \text{ (mg)} = c_0 V_0 W_1 \text{ (mg)} = c_e V_0 q_e \text{ (mg g}^{-1}\text{)} = \frac{w_0 - w_1}{m_0}$$

2.6. Drug Loading

A quantity of 0.6 g of a gelled alginate block was put into a solution containing DOX, calcium chloride, and SF. The concentrations of DOX in the mineralization protocol

were 0.1, 0.2, and 0.5 mg mL⁻¹. After mineralization for a period of 48 h, the alginate block containing DOX-CaCO₃-alginate minerals was weighed (m_{total}) and dissolved in hydrochloric acid (0.1 mol L⁻¹), and the weight of the loaded DOX ($m_{\text{loaded DOX}}$) was tested by an ultraviolet-visible (UV-vis) spectrophotometry method previously. Blank mineral samples were collected directly from a solution that did not contain the alginate block. The DOX loading capacity was calculated according to the following equation:

$$\text{Loading capacity (\%)} = \frac{m_{\text{loaded DOX}}}{m_{\text{total}}} \times 100\%$$

2.7. In Vitro Drug Release

The collected DOX-alginate, DOX-CaCO₃, and DOX-CaCO₃-alginate materials scraped from the glass substrate (1.0 cm × 1.0 cm), each containing 2 mg (m_0) of DOX, were dispersed in 10 mL deionized water with an ultrasound separately. Then, the dispersions were transferred into dialysis tubes (MWCO: 3500 Da), and placed in a conical flask containing a volume of 50 mL (V_0) 0.01 mM PBS buffer at pH 7.4 in dark conditions. The conical flask was oscillated at 100 rpm at 37 °C, where 2 mL (V) of a solution containing DOX released in the conical flask was taken at regular intervals, and equal volumes of fresh PBS buffer solution were supplemented at the same time. The variations in the DOX concentrations over time were measured by the ultraviolet-visible (UV-vis) spectrophotometry method. The cumulative drug release percentages were calculated as follows. The drug release properties of the CaCO₃-SA-DOX samples at different pH values of 7.4, 6.5, and 4.5 were evaluated using the same method:

$$\text{First release percentage} = \frac{c_1 V_0}{m_0} \times 100\% \quad \text{Cumulative release percentage of the } i^{\text{th}} \quad i \geq 2 = \frac{c_i V_0 + V \sum_{i=2}^i c_{i-1}}{m_0} \times 100\%$$

c_i (g L⁻¹): DOX concentrations in buffer solution taken out for the i -th time.

2.8. Characterization

Scanning electron microscopy (SEM) images were collected with a Hitachi S4800 (5 kV acceleration voltage). First, the sample was treated with liquid nitrogen, and then the fractured thin films or the full-face samples were stuck onto double-sided conducting tape. Finally, the samples were coated with a layer of 10 nm of platinum with a JFC-600 sputter coater before characterization. Regarding the DOX-hydrogel samples 333 mL of a 6 mg mL⁻¹ doxorubicin hydrochloride aqueous solution was mixed with 2 mg of a 2 wt% alginate solution under ultrasonication before lyophilization. Optical microscopy (OM) and polarized optical microscopy (POM) images were collected using an Olympus BX53 OM equipped with polarizers. The XRD results were obtained by using an X'pert PRO PANalytical X-ray diffractometer equipped with Cu K α radiation, where the diffraction patterns were generated with the instrument operating at 40 mA and 40 kV with a step size of 0.016°. The Fourier transform infrared (FT-IR) spectra (in the region of 4000–500 cm⁻¹) were recorded by using a Nicolet iS10 spectrometer with the ATR mode in ambient conditions. The ultraviolet-visible (UV-vis) spectra as well as the absorbance test were recorded by using a Perkin Elmer LAMBDA750 spectrometer in ambient conditions. The steady state photoluminescent spectra were measured using a (HITACHI) F-4600 Fluorescence Spectrophotometer, where the excitation wavelength was 450 nm. Fluorescence images were collected using a Leica DM 6000B for fluorescence microscopy and green fluorescence, with a wavelength of 515–560 nm used for excitation.

3. Results and Discussion

In the current study, seeded mineralization [38] was deployed for the precipitation of DOX-CaCO₃-alginate composites. In the primary step, polycrystalline CaCO₃ seeds comprising granular structural units were deposited on a chitosan film in the presence of a polymeric additive: poly(dl-aspartic acid). In a parallel experiment, DOX was dispersed in

a 2.0 wt% alginate hydrogel beforehand at a concentration of 0.2 g L^{-1} . Subsequently, this DOX-alginate solution was spin-coated uniformly on the seed layers for the overgrowth of the prismatic DOX- CaCO_3 -alginate minerals in a mother liquor containing calcium cations (20 mM), silk fibroin ($0.2 \text{ wt}\%$), and DOX (0.2 g L^{-1}). The synergistic occlusion of the DOX-alginate hydrogels led to a high drug load of $0.2 \text{ wt}\%$, while the overgrowth in the hydrogel's absence caused a relatively low occlusion level of $0.04 \text{ wt}\%$. Moreover, the occlusion level of the DOX molecules increased with the concentration of DOX in the reacting mother liquor (Figure 1f). We did not go beyond a concentration of DOX in the mother liquor of 0.5 g L^{-1} because very high drug loads might cause cytotoxicity. Hence, the synergy between DOX and alginate guaranteed high and uniform drug loads in the prismatic DOX- CaCO_3 -alginate minerals.

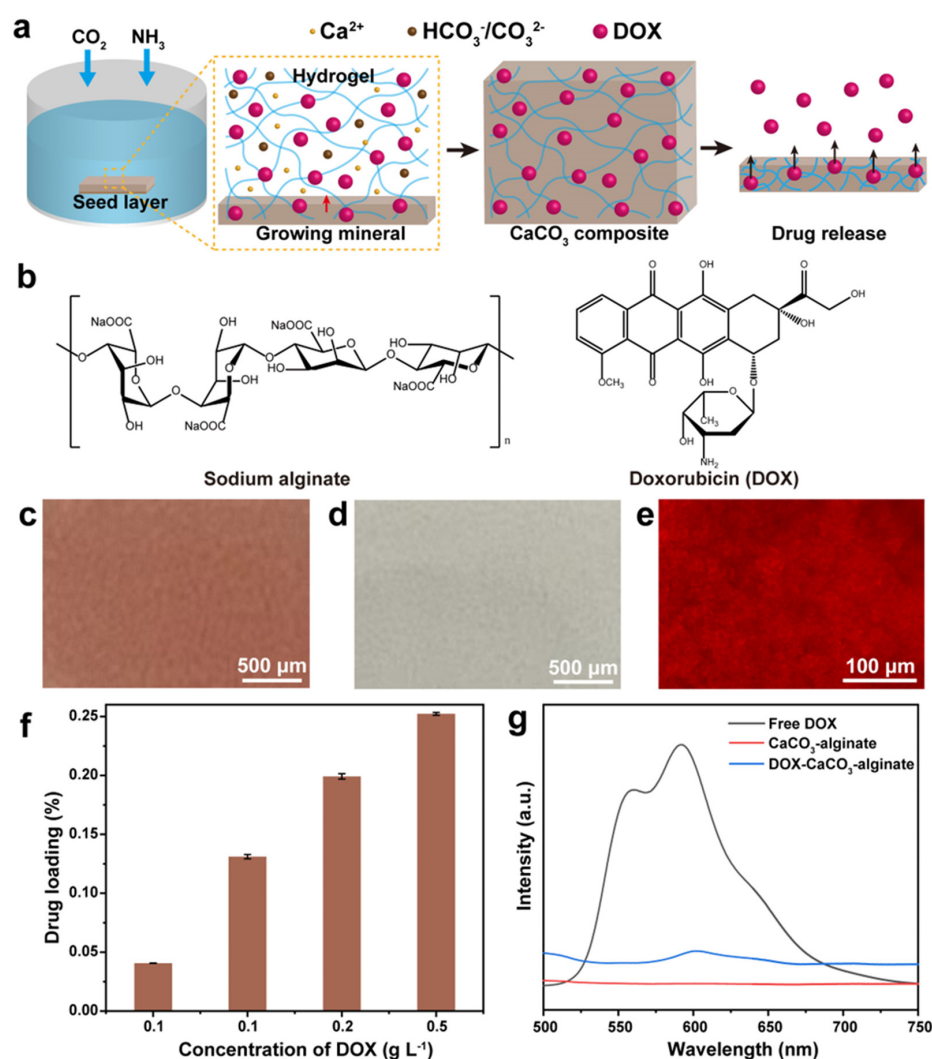


Figure 1. (a) Scheme of the seeded mineralization deployed for the formation of the DOX- CaCO_3 -alginate composite. (b) Molecular formulae of sodium alginate and DOX. (c,d) Digital photos of DOX- CaCO_3 -alginate (c) and CaCO_3 -alginate (d) films. (e) Fluorescence optical microscopic image (green fluorescence with a wavelength of 515–560 nm was used for excitation) of the DOX- CaCO_3 -alginate film. (f) Correlations between the concentration of DOX in the reacting mother liquors and the drug occlusion levels, where all measurements and calculations were based on the UV-vis spectra and the Beer–Lambert law. (g) Steady state photoluminescent spectra (excitation wavelength = 450 nm) of DOX solution, a CaCO_3 -alginate film, and a DOX- CaCO_3 -alginate film.

A polarized optical microscopic (POM) image disclosed the formation of continuous prismatic DOX-CaCO₃-alginate overlayers after the multistep mineralization (Figure S2). Moreover, a digital photo showed the uniform red color of the prismatic mineral (Figure 1c), which hints at the homogeneous spatial distribution of the DOX components. By contrast, the prismatic CaCO₃-alginate films were colorless in the absence of the DOX components (Figure 1d). Under green fluorescence illumination, intensive fluorescence was emitted from the DOX-CaCO₃-alginate overlayers (Figure 1e). A separate steady state photoluminescence spectrum showed emission peaks at 595 nm, which was consistent with that of DOX in the solution (Figure 1g). Moreover, the UV-vis spectroscopy of the DOX-CaCO₃-alginate composite showed absorption peaks of ~233 nm, ~253 nm, and ~500 nm, which were very close to those of the DOX solutions (Figure S4a). The absorption peak of the DOX-CaCO₃-alginate composites was bathochromically shifted by ~20 nm compared with that of the DOX solution, which can be ascribed to the molecular interactions between the DOX and alginate. Therefore, both the photos and the UV-vis spectra indicate that DOX molecules were uniformly occluded in the DOX-CaCO₃-alginate mineral.

Cross-sectional scanning electron microscopy (SEM) was employed to disclose the microstructural characteristics of the prismatic DOX-CaCO₃-alginate overlayers (Figure 2a,b). The overlayer is composed of rhombohedral structural units, where the typical {104} facets are disclosed and observable. The surface of these rhombohedra is not smooth but is highly roughened, which is ascribed to the presence of soluble silk fibroin additives and hydrogel matrices in the course of mineralization. The occurrence of scattered nanofibrils in the overlayer should be attributed to the occluded hydrogel matrices. The rhombohedral structural feature of the DOX-CaCO₃-alginate mineral was in line with that of its CaCO₃ counterpart synthesized in DOX's absence. This result is different from a previous study, which reported that DOX—as a soluble additive—had a direct impact on the morphological control of DOX-CaCO₃ precipitates [13]. Therefore, it was assumed that in the overgrowth process, all DOX molecules intimately associated with the hydrogel matrices were occluded in the mineralized product. The concentration of the free DOX molecules should be low or even ignorable, and therefore, the deployment of DOX had no apparent impact on the morphological outcome of the DOX-CaCO₃-alginate composites. Additionally, the X-ray diffraction pattern confirmed that calcite was the only crystalline polymorph, and no peak belonging to DOX was present (Figure S3).

Gently etching the DOX-CaCO₃-alginate composites with deionized water led to the dissolution of the mineralized constituents on the exterior surface, while both the DOX and alginate hydrogels were preserved, owing to their insolubility in water. The lyophilized surface is featured with the occurrence of the nanofibrillar network, which should be ascribed to the reminiscent DOX-alginate networks (Figure 2c). It is worth noting that no isolated particle was detectable, which indicates the close interactions between the DOX and alginate constituents in the nanofibrillar structure. As a comparison, agglomerating DOX nanoparticles were precipitated in the DOX aqueous solution (Figure 2d). Therefore, the result of the etching treatment suggests that the intimate interactions between the DOX and alginate components and dehydration could not cause the occurrence of phase separation between the two chemicals at the nanoscale. Additionally, all DOX constituents were associated with the hydrogel matrices and occluded in the DOX-CaCO₃-alginate composites.

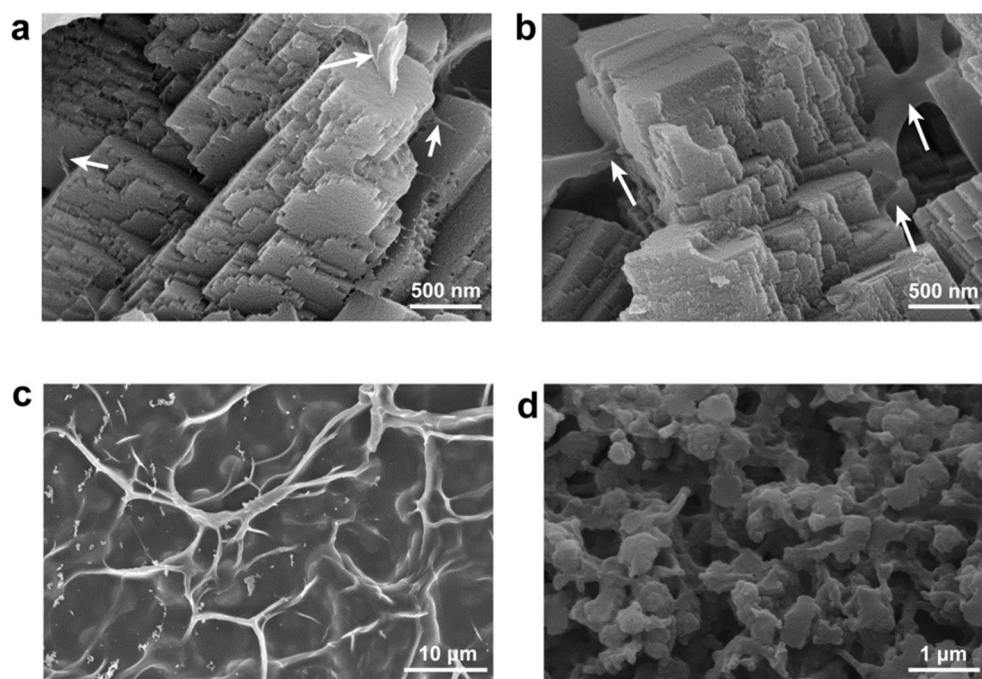


Figure 2. (a,b) Cross-sectional SEM images showing the DOX-CaCO₃-alginate (a) and CaCO₃-alginate (b) films obtained in 2 wt% alginate hydrogel matrices, where the white arrows point to the gel networks embedded in the lyophilized samples. (c) Top-view SEM image showing the appearance of nanofibrillar networks on the exterior surface of the DOX-CaCO₃-alginate overlayers after slight etching with water. (d) SEM image showing DOX powders precipitated in bulk phase.

The DOX-alginate hydrogels were lyophilized to provide a mechanistic understanding of the interactions between the two organic components. The porous scaffold of the lyophilized DOX-alginate hybrid hydrogels was morphologically similar to that of the pristine alginate one (Figure 3a,b). No nanoparticulate structure could be detected on the lyophilized scaffold of the DOX-alginate hybrid, which hints that the DOX constituents can be dispersed in the alginate matrices for the formation of uniform structures. These results are in line with the finding of the etching experiments, both of which confirm that both DOX and alginate components could be occluded in the CaCO₃ matrices in a synergistic manner. In addition to the alginate hydrogels, the uniform nanofibrillar scaffold of the lyophilized DOX-agarose hydrogels could be formed via the same protocol, which suggests that DOX exhibits the capability of formation of uniform nanofibrous structures with multiple polymeric candidates (Figure 3c,d). The molecular interactions between DOX and the polymers can be evaluated with the adsorption isotherm. The adsorption capacities of the alginate and agarose hydrogels (2.0 wt%) were as high as ~31 mg g⁻¹ and ~36 mg g⁻¹, respectively (Figure 3e). It is determined that the carboxyl and hydroxyl groups on both types of polymeric chains can interact with amine and hydroxyl groups on DOX. The deployment of DOX-alginate hydrogels led to a high drug load of 0.25 wt%, which eventually caused a DOX occlusion level of 0.04 wt% in the DOX-CaCO₃-alginate composites. In short, the intermolecular interactions between DOX and alginate guaranteed high and uniform drug loads in the prismatic CaCO₃ minerals.

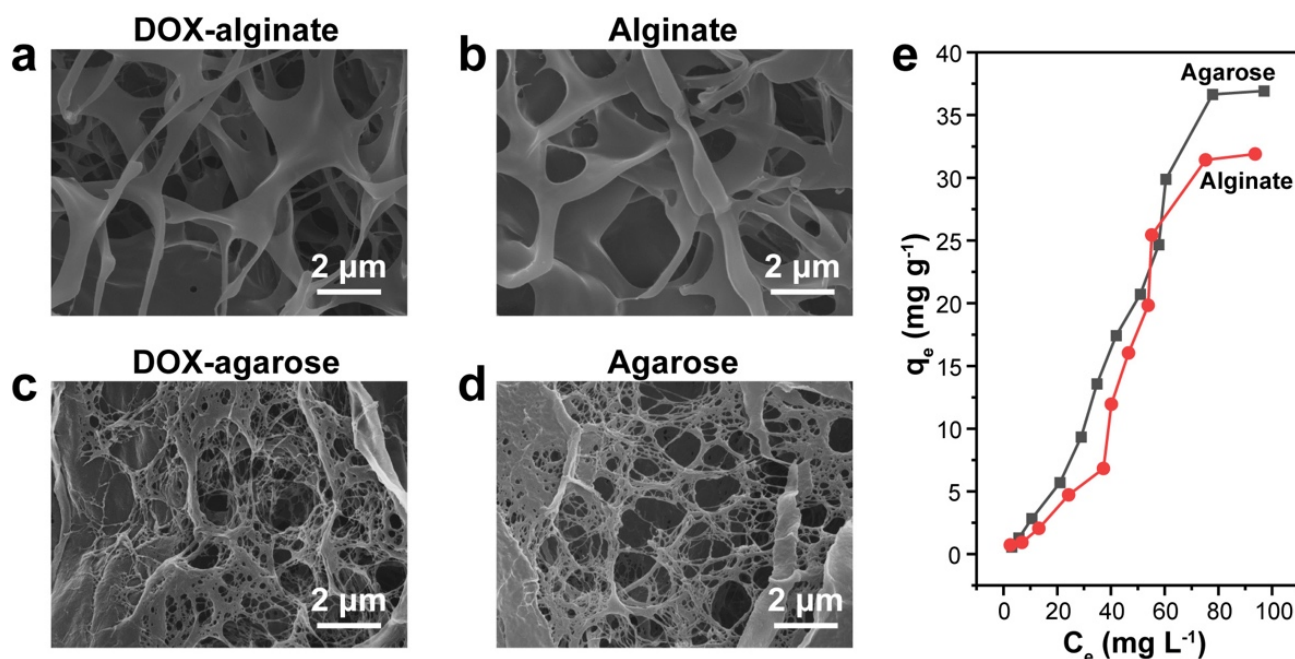


Figure 3. (a,b) SEM images of lyophilized DOX-alginate (a) and alginate (b) hydrogels, where the concentrations of DOX and alginate were 2 g L^{-1} and 2 wt%, respectively. (c,d) SEM images of lyophilized DOX—agarose (c) and agarose (d) hydrogels, where the concentrations of DOX and agarose were 2 g L^{-1} and 2 wt%, respectively. (e) Adsorption isotherms of DOX molecules with lyophilized alginate and agarose hydrogels (2 wt%).

Synergistic occlusion of the DOX constituents should cause sustained drug release of the DOX- CaCO_3 -alginate hybrids. In vitro release studies of the target composite, together with DOX-alginate hydrogels and the DOX- CaCO_3 hybrid mineral, (DOX was passively occluded from the bulk phase instead of using alginate hydrogels.) were conducted using a dialytic technique. All samples were assayed using UV-vis spectrophotometry at a wavelength of 480 nm. All hybrids exhibited a sustained release performance throughout the period, among which the DOX- CaCO_3 -alginate hybrids showed the best performance. Meanwhile, both the physical embedding in the mineralized matrix and the molecular association with nanofibrillar alginate constituents led to a reduction in the initial burst release and the subsequent steady release performance, as can be found in the comparison of releasing patterns. It is also worth noting that alginate—a natural polysaccharide—is a type of excellent biomacromolecule with excellent biocompatibility and biodegradability.

Next, the in vitro drug release behaviors of the DOX- CaCO_3 -alginate hybrids at different pH values were evaluated, as the CaCO_3 mineral itself is a typical pH-responsive drug carrier. Three aqueous solutions with pH values of 7.4, 6.5, and 4.5 were selected to simulate the physiological condition, the mild tumor microenvironment condition, and the significant acidic tumor microenvironment condition, respectively. After a releasing period of 48 h, a proportion of 56 wt% DOX molecules from the composites was released into the pH = 4.5 solution, which was significantly higher than those released into the relatively basic solutions (Figure 4b). Thus, this pH-triggered sustained and controlled release of the DOX constituents may facilitate targeted drug release in the acidic tumor environment within tumor cells and, in the meantime, reduce the side effects for normal cells under physiological conditions.

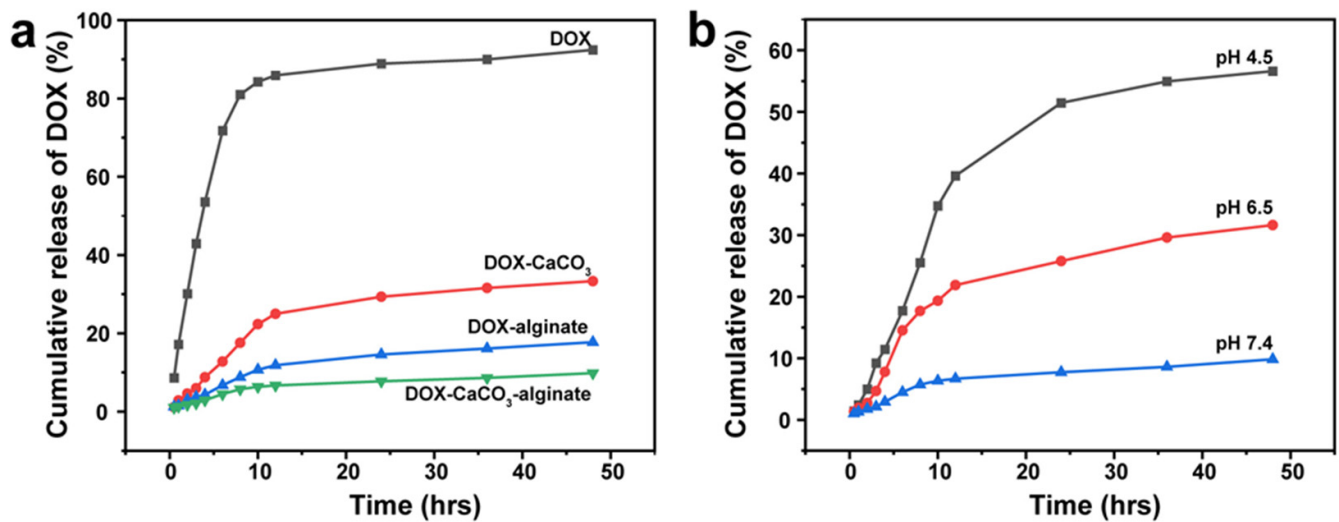


Figure 4. (a) In vitro cumulative release of the DOX components at pH 7.4 using DOX-CaCO₃-alginate, DOX-alginate, DOX-CaCO₃ composites, and DOX powders. (b) In vitro cumulative DOX release of the DOX components in the DOX-CaCO₃-alginate composites at different pH values.

4. Conclusions

The strategy of synergistic occlusion was successful in the design of DOX-CaCO₃-alginate hybrid composites with sustained drug delivery properties. The formation of a molecular solution between DOX and the alginate hydrogel guarantees synergistic occlusion in the course of prismatic mineralization. The composites exhibited sustained drug release performance, which was ascribed to the physical occlusion in the CaCO₃ mineral and the intimate interactions between DOX and the nanofibrillar alginate. In principle, there exist many drug-hydrogel pairs that can form molecular solutions in the proper experimental conditions. It is therefore deemed that this emerging strategy can be a general approach to the design of smart drug delivery systems.

Supplementary Materials: The following supporting information can be downloaded at <https://www.mdpi.com/article/10.3390/cryst13010132/s1>: The experimental section; Figure S1: molecular formula of agarose; Figure S2: polarized optical microscopic images of CaCO₃-alginate and DOX-CaCO₃-alginate; Figure S3: XRD patterns of the DOX-CaCO₃-alginate composites; Figure S4: UV-vis spectra of DOX containing compounds; and the standard curve of DOX absorbance at 480 nm (PDF).

Author Contributions: Conceptualization, Y.J.; methodology, Y.J.; investigation, Y.-X.L.; writing—original draft preparation, Y.-X.L.; writing—review and editing, Y.J.; visualization, Y.J.; supervision, Y.J.; project administration, Y.J.; funding acquisition, Y.J. All authors have read and agreed to the published version of the manuscript.

Funding: This research was funded by the Natural Science Foundation of China (21875193 and 22075235).

Data Availability Statement: All authors have confirmed that no new data were created.

Acknowledgments: Zhongxiong Fan, Zhenqing Hou, Zheng-Zheng Li, Xiang-Dong Liu, Xin-Xin Liu, Xin-Yu Liu, Chun-Xiao Song, Si-Si Song, Yange Wang, Li-Kun Yang, and Xiuming Zhang are acknowledged for their experimental assistance.

Conflicts of Interest: The authors declare no conflict of interest.

References

1. Ferreira, A.M.; Vikulina, A.S.; Volodkin, D. CaCO₃ crystals as versatile carriers for controlled delivery of antimicrobials. *J. Control. Release* **2020**, *328*, 470–489. [[CrossRef](#)] [[PubMed](#)]
2. Ueno, Y.; Futagawa, H.; Takagi, Y.; Ueno, A.; Mizushima, Y. Drug-incorporating calcium carbonate nanoparticles for a new delivery system. *J. Control. Release* **2005**, *103*, 93–98. [[CrossRef](#)] [[PubMed](#)]
3. Maleki Dizaj, S.; Barzegar-Jalali, M.; Zarrintan, M.H.; Adibkia, K.; Lotfipour, F. Calcium carbonate nanoparticles as cancer drug delivery system. *Expert Opin. Drug Deliv.* **2015**, *12*, 1649–1660. [[CrossRef](#)] [[PubMed](#)]
4. Dong, Z.; Feng, L.; Zhu, W.; Sun, X.; Gao, M.; Zhao, H.; Chao, Y.; Liu, Z. CaCO₃ nanoparticles as an ultra-sensitive tumor-pH-responsive nanoplatform enabling real-time drug release monitoring and cancer combination therapy. *Biomaterials* **2016**, *110*, 60–70. [[CrossRef](#)] [[PubMed](#)]
5. Peng, C.; Zhao, Q.; Gao, C. Sustained delivery of doxorubicin by porous CaCO₃ and chitosan/alginate multilayers-coated CaCO₃ microparticles. *Colloids Surf. A* **2010**, *353*, 132–139. [[CrossRef](#)]
6. Wang, J.; Chen, J.-S.; Zong, J.-Y.; Zhao, D.; Li, F.; Zhuo, R.-X.; Cheng, S.-X. Calcium Carbonate/Carboxymethyl Chitosan Hybrid Microspheres and Nanospheres for Drug Delivery. *J. Phys. Chem. C* **2010**, *114*, 18940–18945. [[CrossRef](#)]
7. Parakhonskiy, B.V.; Haase, A.; Antolini, R. Sub-Micrometer Vaterite Containers: Synthesis, Substance Loading, and Release. *Angew. Chem. Int. Ed.* **2012**, *51*, 1195–1197. [[CrossRef](#)]
8. Manabe, K.; Oniszcuk, J.; Michely, L.; Belbekhouche, S. pH- and redox-responsive hybrid porous CaCO₃ microparticles based on cyclodextrin for loading three probes all at once. *Colloids Surf. A* **2020**, *602*, 125072. [[CrossRef](#)]
9. Zhao, Y.; Lu, Y.; Hu, Y.; Li, J.-P.; Dong, L.; Lin, L.-N.; Yu, S.-H. Synthesis of Superparamagnetic CaCO₃ Mesocrystals for Multistage Delivery in Cancer Therapy. *Small* **2010**, *6*, 2436–2442. [[CrossRef](#)]
10. Wei, W.; Ma, G.-H.; Hu, G.; Yu, D.; McLeish, T.; Su, Z.-G.; Shen, Z.-Y. Preparation of Hierarchical Hollow CaCO₃ Particles and the Application as Anticancer Drug Carrier. *J. Am. Chem. Soc.* **2008**, *130*, 15808–15810. [[CrossRef](#)]
11. Dong, Z.; Feng, L.; Hao, Y.; Chen, M.; Gao, M.; Chao, Y.; Zhao, H.; Zhu, W.; Liu, J.; Liang, C.; et al. Synthesis of Hollow Biomineralized CaCO₃-Polydopamine Nanoparticles for Multimodal Imaging-Guided Cancer Photodynamic Therapy with Reduced Skin Photosensitivity. *J. Am. Chem. Soc.* **2018**, *140*, 2165–2178. [[CrossRef](#)]
12. Lowenstam, H.A.; Weiner, S. *On Biomineralization*; Oxford University Press: Oxford, UK, 1989.
13. Magnabosco, G.; Giosia, M.D.; Polishchuk, I.; Weber, E.; Fermani, S.; Bottoni, A.; Zerbetto, F.; Pelicci, P.G.; Pokroy, B.; Rapino, S.; et al. Calcite Single Crystals as Hosts for Atomic-Scale Entrapment and Slow Release of Drugs. *Adv. Healthc. Mater.* **2015**, *4*, 1510–1516. [[CrossRef](#)]
14. Kim, Y.-Y.; Carloni, J.D.; Demarchi, B.; Sparks, D.; Reid, D.G.; Kunitake, M.E.; Tang, C.C.; Duer, M.J.; Freeman, C.L.; Pokroy, B.; et al. Tuning hardness in calcite by incorporation of amino acids. *Nat. Mater.* **2016**, *15*, 903–910. [[CrossRef](#)]
15. Lang, A.; Mijowska, S.; Polishchuk, I.; Fermani, S.; Falini, G.; Katsman, A.; Marin, F.; Pokroy, B. Acidic Monosaccharides become Incorporated into Calcite Single Crystals. *Chem. Eur. J.* **2020**, *26*, 16860–16868. [[CrossRef](#)]
16. Kulak, A.N.; Iddon, P.; Li, Y.; Armes, S.P.; Cölfen, H.; Paris, O.; Wilson, R.M.; Meldrum, F.C. Continuous Structural Evolution of Calcium Carbonate Particles: A Unifying Model of Copolymer-Mediated Crystallization. *J. Am. Chem. Soc.* **2007**, *129*, 3729–3736. [[CrossRef](#)]
17. Kim, Y.-Y.; Darkins, R.; Broad, A.; Kulak, A.N.; Holden, M.A.; Nahi, O.; Armes, S.P.; Tang, C.C.; Thompson, R.F.; Marin, F.; et al. Hydroxyl-rich macromolecules enable the bio-inspired synthesis of single crystal nanocomposites. *Nat. Commun.* **2019**, *10*, 5682. [[CrossRef](#)]
18. Natalio, F.; Corrales, T.P.; Panthöfer, M.; Schollmeyer, D.; Lieberwirth, I.; Müller, W.E.G.; Kappl, M.; Butt, H.-J.; Tremel, W. Flexible Minerals: Self-Assembled Calcite Spicules with Extreme Bending Strength. *Science* **2013**, *339*, 1298–1302. [[CrossRef](#)]
19. Kim, Y.-Y.; Ganesan, K.; Yang, P.; Kulak, A.N.; Borukhin, S.; Pechook, S.; Ribeiro, L.; Kröger, R.; Eichhorn, S.J.; Armes, S.P.; et al. An artificial biomineral formed by incorporation of copolymer micelles in calcite crystals. *Nat. Mater.* **2011**, *10*, 890–896. [[CrossRef](#)]
20. Ning, Y.; Han, L.; Derry, M.J.; Meldrum, F.C.; Armes, S.P. Model Anionic Block Copolymer Vesicles Provide Important Design Rules for Efficient Nanoparticle Occlusion within Calcite. *J. Am. Chem. Soc.* **2019**, *141*, 2557–2567. [[CrossRef](#)]
21. Giosia, M.D.; Polishchuk, I.; Weber, E.; Fermani, S.; Pasquini, L.; Pugno, N.M.; Zerbetto, F.; Montalti, M.; Calvaresi, M.; Falini, G.; et al. Bioinspired Nanocomposites: Ordered 2D Materials Within a 3D Lattice. *Adv. Funct. Mater.* **2016**, *26*, 5569–5575. [[CrossRef](#)]
22. Meldrum, F.C.; Cölfen, H. Controlling Mineral Morphologies and Structures in Biological and Synthetic Systems. *Chem. Rev.* **2008**, *108*, 4332–4432. [[CrossRef](#)] [[PubMed](#)]
23. Weber, E.; Pokroy, B. Intracrystalline inclusions within single crystalline hosts: From biomineralization to bio-inspired crystal growth. *CrystEngComm* **2015**, *17*, 5873–5883. [[CrossRef](#)]
24. Barbalinardo, M.; Di Giosia, M.; Polishchuk, I.; Magnabosco, G.; Fermani, S.; Biscarini, F.; Calvaresi, M.; Zerbetto, F.; Pellegrini, G.; Falini, G.; et al. Retinoic acid/calcite micro-carriers inserted in fibrin scaffolds modulate neuronal cell differentiation. *J. Mater. Chem. B* **2019**, *7*, 5808–5813. [[CrossRef](#)] [[PubMed](#)]
25. Pokroy, B.; Fitch, A.N.; Marin, F.; Kapon, M.; Adir, N.; Zolotoyabko, E. Anisotropic lattice distortions in biogenic calcite induced by intra-crystalline organic molecules. *J. Struct. Biol.* **2006**, *155*, 96–103. [[CrossRef](#)]
26. Weiner, S.; Addadi, L. Crystallization Pathways in Biomineralization. *Annu. Rev. Mater. Res.* **2011**, *41*, 21–40. [[CrossRef](#)]

27. Addadi, L.; Joester, D.; Nudelman, F.; Weiner, S. Mollusk shell formation: A source of new concepts for understanding biomineralization processes. *Chem. Eur. J.* **2006**, *12*, 981–987. [[CrossRef](#)]
28. Ritchie, R.O. The conflicts between strength and toughness. *Nat. Mater.* **2011**, *10*, 817–822. [[CrossRef](#)]
29. Levi-Kalisman, Y.; Falini, G.; Addadi, L.; Weiner, S. Structure of the Nacreous Organic Matrix of A Bivalve Mollusk Shell Examined in the Hydrated State Using Cryo-TEM. *J. Struct. Biol.* **2001**, *135*, 8–17. [[CrossRef](#)]
30. Calvaresi, M.; Di Giosia, M.; Ianiro, A.; Valle, F.; Fermani, S.; Polishchuk, I.; Pokroy, B.; Falini, G. Morphological changes of calcite single crystals induced by graphene–biomolecule adducts. *J. Cryst. Growth* **2017**, *457*, 356–361. [[CrossRef](#)]
31. Weber, E.; Bloch, L.; Guth, C.; Fitch, A.N.; Weiss, I.M.; Pokroy, B. Incorporation of a Recombinant Biomineralization Fusion Protein into the Crystalline Lattice of Calcite. *Chem. Mater.* **2014**, *26*, 4925–4932. [[CrossRef](#)]
32. Marzec, B.; Green, D.C.; Holden, M.A.; Coté, A.S.; Ihli, J.; Khalid, S.; Kulak, A.; Walker, D.; Tang, C.; Duffy, D.M.; et al. Amino Acid Assisted Incorporation of Dye Molecules within Calcite Crystals. *Angew. Chem. Int. Ed.* **2018**, *57*, 8623–8628. [[CrossRef](#)] [[PubMed](#)]
33. Asenath-Smith, E.; Li, H.; Keene, E.C.; Seh, Z.W.; Estroff, L.A. Crystal Growth of Calcium Carbonate in Hydrogels as a Model of Biomineralization. *Adv. Funct. Mater.* **2012**, *22*, 2891–2914. [[CrossRef](#)]
34. Liu, Y.; Yuan, W.; Shi, Y.; Chen, X.; Wang, Y.; Chen, H.; Li, H. Functionalizing Single Crystals: Incorporation of Nanoparticles Inside Gel-Grown Calcite Crystals. *Angew. Chem. Int. Ed.* **2014**, *53*, 4127–4131. [[CrossRef](#)] [[PubMed](#)]
35. Kim, Y.-Y.; Schenk, A.S.; Walsh, D.; Kulak, A.N.; Cespedes, O.; Meldrum, F.C. Bio-inspired formation of functional calcite/metal oxide nanoparticle composites. *Nanoscale* **2014**, *6*, 852–859. [[CrossRef](#)]
36. Liu, Y.; Zang, H.; Wang, L.; Fu, W.; Yuan, W.; Wu, J.; Jin, X.; Han, J.; Wu, C.; Wang, Y.; et al. Nanoparticles Incorporated inside Single-Crystals: Enhanced Fluorescent Properties. *Chem. Mater.* **2016**, *28*, 7537–7543. [[CrossRef](#)]
37. Rockwood, D.N.; Preda, R.C.; Yücel, T.; Wang, X.; Lovett, M.L.; Kaplan, D.L. Materials fabrication from Bombyx mori silk fibroin. *Nat. Protoc.* **2011**, *6*, 1612–1631. [[CrossRef](#)]
38. Li, M.; Chen, Y.; Mao, L.-B.; Jiang, Y.; Liu, M.-F.; Huang, Q.; Yu, Z.; Wang, S.; Yu, S.-H.; Lin, C.; et al. Seeded Mineralization Leads to Hierarchical CaCO₃ Thin Coatings on Fibers for Oil/Water Separation Applications. *Langmuir* **2018**, *34*, 2942–2951. [[CrossRef](#)]
39. Wang, D.; Feng, Y.-X.; Li, M.; Guo, S.; Jiang, Y. Seeded Mineralization in Silk Fibroin Hydrogel Matrices Leads to Continuous Rhombohedral CaCO₃ Films. *Crystals* **2020**, *10*, 166. [[CrossRef](#)]

Disclaimer/Publisher’s Note: The statements, opinions and data contained in all publications are solely those of the individual author(s) and contributor(s) and not of MDPI and/or the editor(s). MDPI and/or the editor(s) disclaim responsibility for any injury to people or property resulting from any ideas, methods, instructions or products referred to in the content.